The H^+ detector is a scintillator mounted in vacuum coupled to a phototube outside the vacuum through an optical feedthrough. A major problem with this detector is that a low efficiency in light collection prevents the observation of single hits. A new design with a better light collection efficiency is underway.

ii. Ion Beam Monitors

Three separate, yet complimentary, devices are used to monitor the beam current. The first is a massive Faraday cup, 700 kg of graphite, capable of completely stopping all the protons in the beam. The charge collected by the cup is drained off using an teflon insulated wire. This device has a slow response time and therefore is not useful for providing information on the instantaneous current. However, the Faraday cup integrates the beam current to arrive at a reliable total charge delivered by the beam. The H^- beam goes through several Havar vacuum windows before reaching the Faraday cup and is stripped down to protons. The output of the Faraday cup is digitized by a NIM current digitizer which produces a TTL logic pulse for every 10^{-14}, on the 100 pA scale, coulombs of charge integrated. This signal is used to normalize each angle or step to the beam current.

The second piece of equipment looking at the beam current is the fast ion chamber with a response time of few μseconds. Briefly, the detector is a cylindrical chamber with two Havar windows on the flat sides. Inside, there are two thin steel plates with a voltage of +1000 volts on the them. The chamber is filled with hydrogen gas kept at a pressure slightly higher than the atmospheric pressure. Once the beam goes through the gas, it collisionally detaches electrons from the hydrogen atoms which are collected by one of the plates. The signal is amplified and then converted to a pulse train by a voltage-to-frequency module. The frequency of the pulse train is proportional to the voltage of the input pulse. This is recorded by the computer keeping track of macropulse intensity fluctuations.

The response time of the fast ion chamber is too slow to resolve individual micropulses even when they are separated by four μseconds. The "paddle" is a square piece of plastic scintillator (4" x 4" x 0.2") mounted on a phototube via a fish tail light guide. The fast pulses produced by the paddle have a FWHM of about 20 ns which enables it to resolve individual micropulses as long as they are separated by more than 20 ns. This allows one to accurately lock the laser trigger to the microstructure. However, the five ns microstructure is smeared by the time response of the detector. Furthermore, the individual micropulse intensity information is not reliable since the scintillator material, or the photocathode, may be saturated by the great number of protons that hit a small area simultaneously. A Cerenkov detection system combined with a fast phototube should provide for an improved timing resolution and a more reliable micropulse intensity measurement. The last point is specially important since a significant portion of our data fluctuations is attributed to micropulse intensity variations from one laser pulse to next.

iii. Laser Beam Monitors

The average laser intensity is measured by a calorimeter located inside the scattering chamber. The calorimeter signal is readout by a power meter through a vacuum BNC feedthrough. The DC analog output of the power meter is sent to the counting house where a 12-bit high impedance ADC polls it at 250 μ seconds after each laser shot. A second calorimeter is mounted on an air actuator outside the scattering chamber. The power meter readout is checked visually by a camera whenever the calorimeter is inserted into the laser beam. A fast photodiode is used to detect the presence of the short laser pulses. This pulse is used to open the ADC gates and to generate an event for the computer. The intensity of the short pulses are measured with a fast vacuum photodiode with a rise time of less than one ns. This allows one to check for any spikes in the temporal profile of the laser pulse

which should be a gaussian under normal operating conditions. The laser trigger is used to start a TDC module which is stopped by the fast photodiode signal. Finally, the signal is digitized by an integrating ADC to keep track of laser pulse intensity outside the chamber.

APPENDIX 8

Hardware

The beam line configurations for the 1988 and 1989 experiments are shown in figures A8.1, A8.2, and A8.3. Some of the pieces of hardware such as the little chamber, big chamber, bending magnets, long skinny magnet, and the electron spectrometer have been in use by the H^- group at LAMPF for some time. A detailed description of these devices are found in the earlier dissertations (Sharifian, Tootoonchi, Frost, Stewart). The recent modifications made to some of these equipment are discussed in Harris's dissertation. Here, we limit the discussion to the new equipment relevant to the foil experiments.

i. The Sliding Foil Changer

The schematic for the sliding foil holder is shown in figure A8.4. The device basically works like a linear slide changer. The slides, each holding one foil, are all placed in the grooves in the slide magazine inside the vacuum chamber. A mechanical vacuum feedthrough and a system of gears is used to couple a stepper motor to the slide holder, moving it along the beam direction. This positions a slide in front of a brass arm which pushes the slide into the beam. A second stepper motor is used, through a vacuum feedthrough and a system of gears, to move the arm in and out of the beam. The arm has a hook that couples to the slide allowing the arm to retrieve the slide. The hook is released once the arm is pulled back to the out limit. A number of limit switches are used to mark the motional limits of the slide holder and the arm. An extra limit switch disables the stepper motor moving the slide holder once a foil is moved out of its retracted position. Each stepper motor is connected to a one-turn precision potentiometer via an appropriate gear. This system allows to know the positions of the slide holder, hence slide identity,

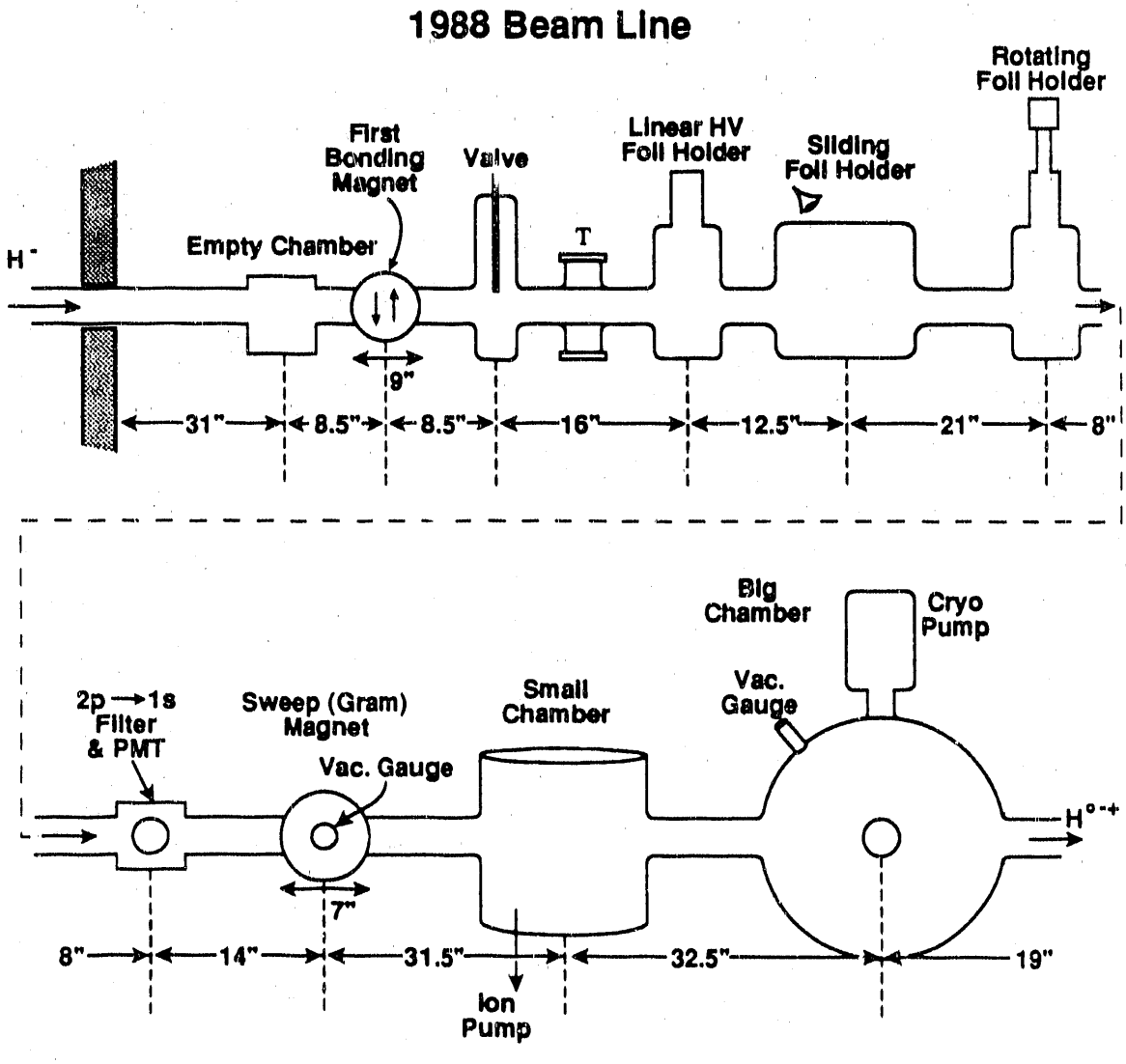

Figure A8.1 Schematic diagram of 1988 beam line, more on the next figure.

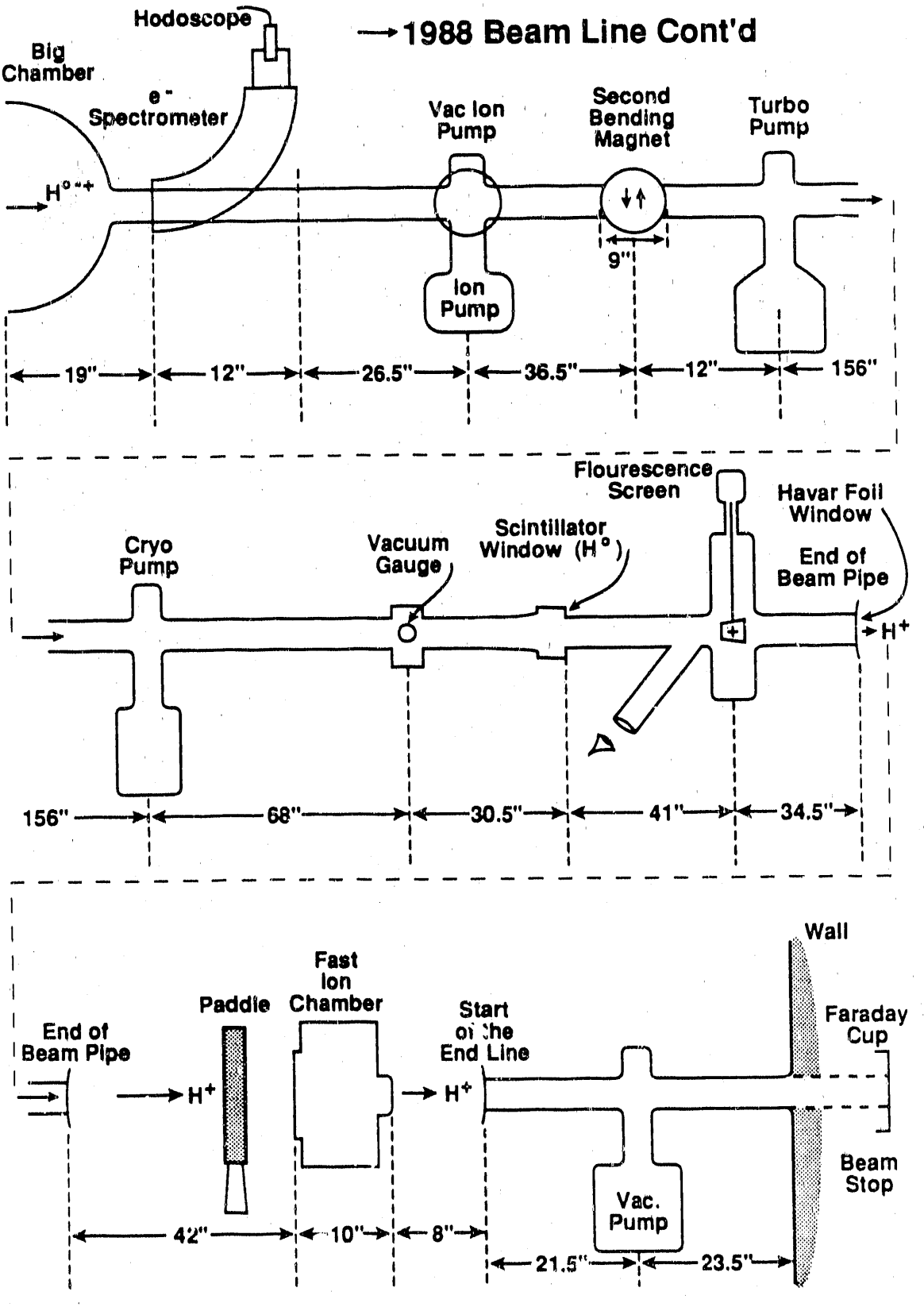

Figure A8.2 1988 beam line continued.

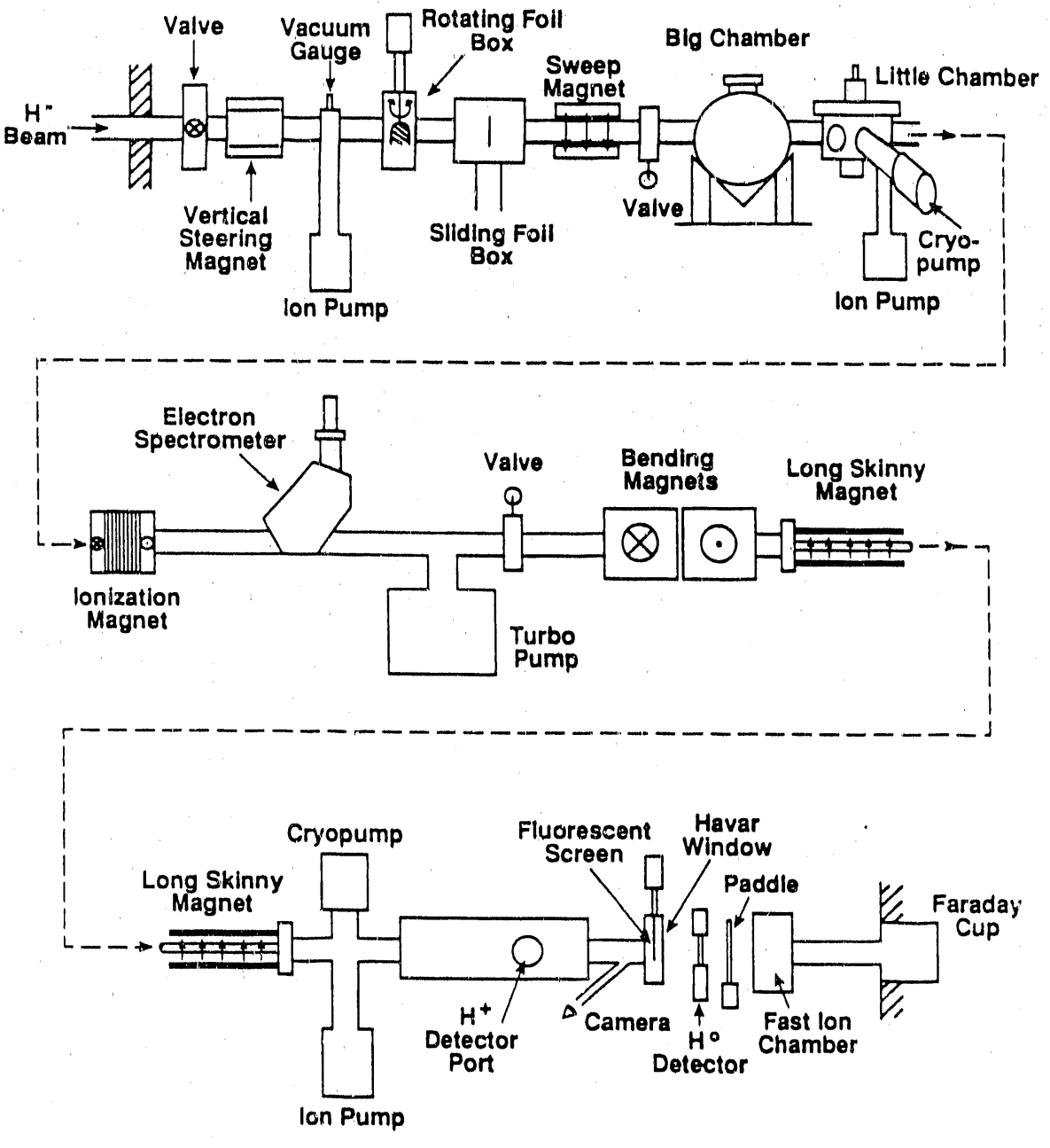

Figure A8.3 Schematic diagram of 1989 beam line.

and the brass arm. The voltage on each potentiometer varies from 0 to 10 volts over the entire range of each component. The slide holder magazine is calibrated against the potentiometer reading for the position of each slide. This calibration is used to position each foil accurately in front of the brass arm for insertion into the beam.

The slides are made of copper as shown in figure A8.4. Each slide is made out of two identical plates that are held together with four flat head screws. An aluminized mylar sheet is stretched over a vacuum table, and a section of the stretched mylar is sandwiched between the two plates. The extra mylar is cutoff and an elliptical hole (1.5cm x 0.5cm) in the middle of the mylar is cut by a laser. The laser cutting insures smooth edges around the elliptical clearance. The slide holder can hold as many as twenty slides where seventeen are used to mount the carbon foils, one is used to mount a fluorescence screen, and the last available slot is used for a cross hair to align the chamber. The foils and the fluorescence screen are observed by a camera looking through a one-inch-thick plexiglass on top of the chamber. Thus, the status of the foils can be checked periodically, and the fluorescence screen is specially useful to make sure that the beam goes through the center of the foil.

The carbon foils are evaporated in vacuum[61] from spectrographically pure graphite. The impurities, for a 20 $\mu g/cm^2$ foil, consist of about 1 atomic percent oxygen, 0.1 atomic percent sodium, a few atomic percent hydrogen, and 100 ppm levels of metallic impurities. The foil thicknesses are measured by the manufacturer using an optical method with an accuracy of $\pm 10\%$. The thin carbon foils ($\leq$ 150 $\mu g/cm^2$) are mounted by floating them in distilled water and then picking them up with the slide. The foil sticks to the surface of the mylar sheet in the slide. The carbon foils are strong enough to support their weight over the exposed elliptical area. The thicker foils are baked first to release their residual stress and then mounted using the above method. Some of the thickest foils are glued to a slide with a vacuum compatible glue.

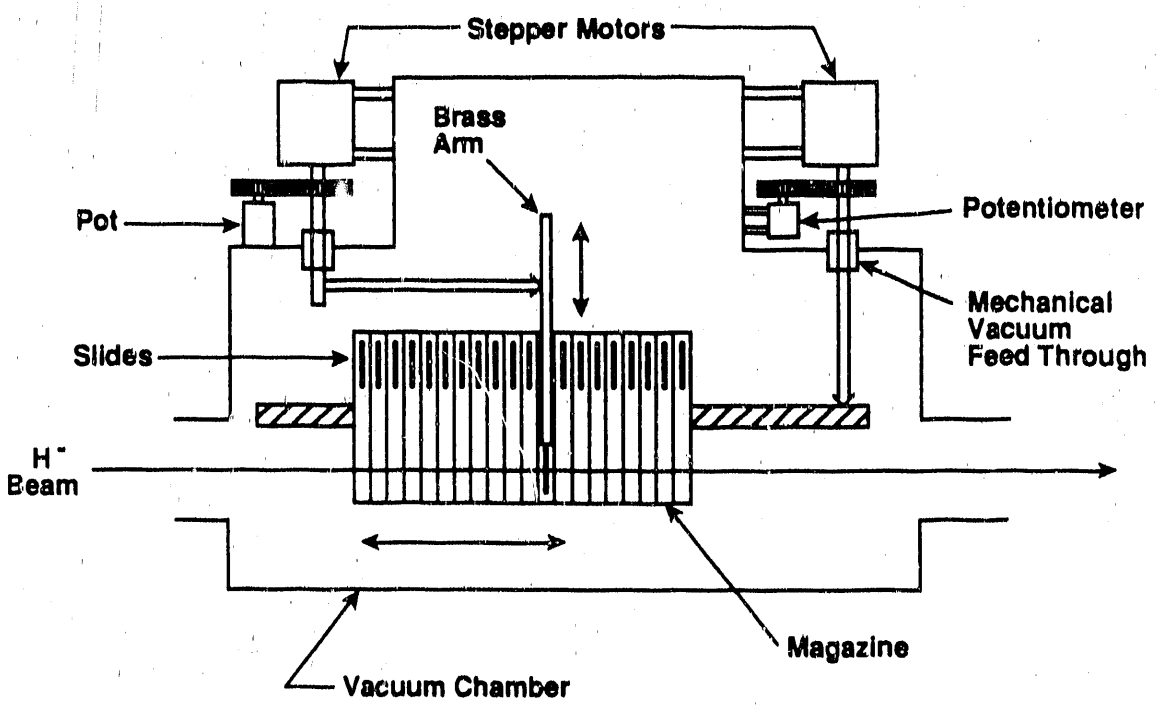

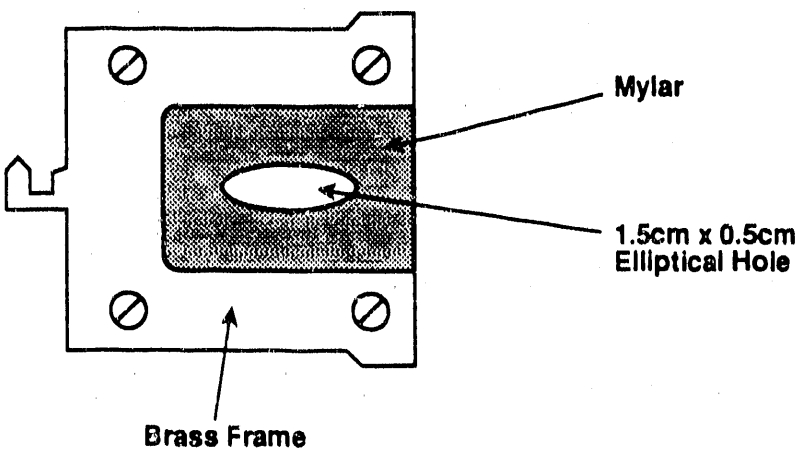

Figure A8.4 Schematic diagram of the sliding foil-holder and the copper slides.

The Rotating Foil Holder

The Rotating foil holder consists of an aluminum slide with a circular opening of one inch in diameter. The slide is mounted on the vacuum end of an actuator that moves the foil in a direction perpendicular to the beam line. A second actuator rotates the foil as to change the angle between the plane of the foil and the H^- beam. The angle can be changed from 0° (i.e. H^- beam at normal incidence to the foil surface) to 40°. As before, two potentiometers keep track of the linear and angular positions of the foil. The angle of the foil is calibrated by reflecting a HeNe laser beam off the surface. The graph of the measured angle versus the potentiometer voltage is shown in figure A8.5. The angle θ as a function of pot voltage is given by

$$\theta = m \times V + b, \tag{A8.1}$$

$$m = -0.36 \pm 0.47 \ degree,$$

$$b = 8.11 \pm 0.09 \ \frac{degree}{volt},$$

where V is the potentiometer readout in volts. This relationship is valid from 0.5 volts to 9.5 volts.

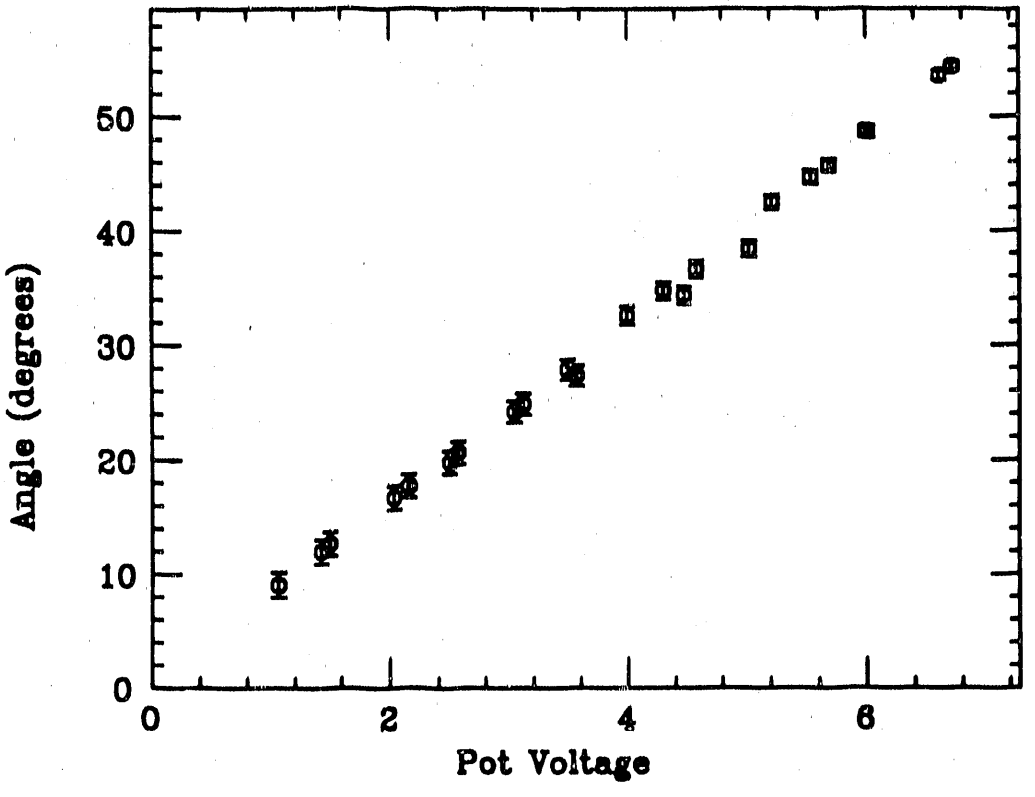

Figure A8.5 The measured tilt angle of the tilting foil-holder versus the pot reading in the counting house.

APPENDIX 9

Measurement of Carbon Foil Thicknesses

The thicknesses of the carbon foils are measured by detecting the energy loss of α particles going through the foils. The experimental setup is shown in figure A9.1. A source of energetic α particles, $^{241}_{95}Am$, is placed at a distance of 20.0 cm away from a solid state detector within the sliding chamber. A foil is inserted at the midpoint between the source and the detector of 1.0 cm in diameter. The vacuum within the chamber is kept at about 10^{-5} torr where there is no detectable loss of energy due to collisions with the residual gas. Once an α particle is incident on the silicon detector a quantity of charge is released which is integrated by the preamp. The result is a step pulse with a long tail retrieved through a 93 Ω BNC connector. The pulse is further amplified by a shaping amplifier producing a gaussian pulse. Finally, an energy spectrum is formed by a MultiChannel Analyzer (MCA) board installed within an IBM-PC.

The MCA is calibrated by using the $^{241}_{95}Am$ and $^{252}_{98}Cf$ sources. Figure A9.2 shows the energy spectrum taken with both sources in place. The first source, $^{241}_{95}Am$, has a primary peak at an energy of 5485.7 keV and a secondary peak at 5443.0 keV. The second source has a major peak at 6118.0 keV and a minor peak at 6076.0 keV. The experimental energy resolution of about 30 keV is not good enough to completely separate the major and minor peaks. The effect is that a shoulder develops on the low energy side of each peak as seen from figure A9.3. The Cf source is taken out for the thickness measurements. A foil is placed at the midpoint between the detector and the source and the resulting shift in energy of the Am source is measured. The measured energy loss of the α particles combined with the expected energy loss per unit carbon foil thickness, 0.717 $\frac{keV}{\mu g/cm^2}$ for the major α particles from the Am source, is used to calculate the thickness of the foil.

Figure A9.4 shows the result of the measurements where the x-axis is the nominal foil thickness and the y-axis is the measured thickness. The horizontal error bars are the uncertainty claimed by the manufacturer. The overall agreement between the nominal and experimentally measured thicknesses are good with a reduced χ^2 of 1.45 resulting in a confidence level of 27.0%. One of the major problems encountered is a drift in the position of the original peak as a function of time, making it necessary to recalibrate the MCA frequently. This technique can be further improved by using a cooled silicon detector to achieve a better energy resolution.

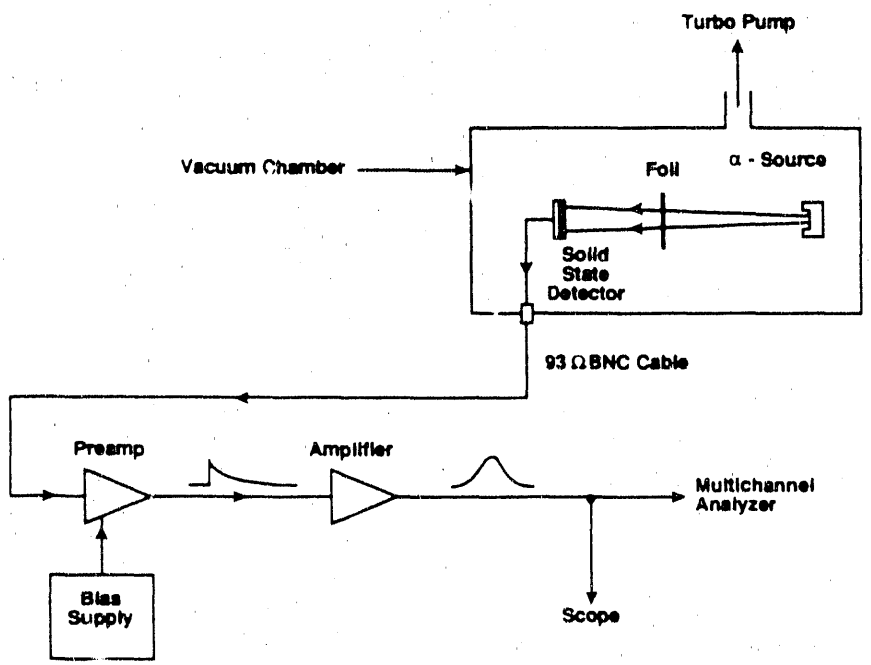

Figure A9.1 Experimental setup of the α-ranging experiment to measure the carbon foil thicknesses.

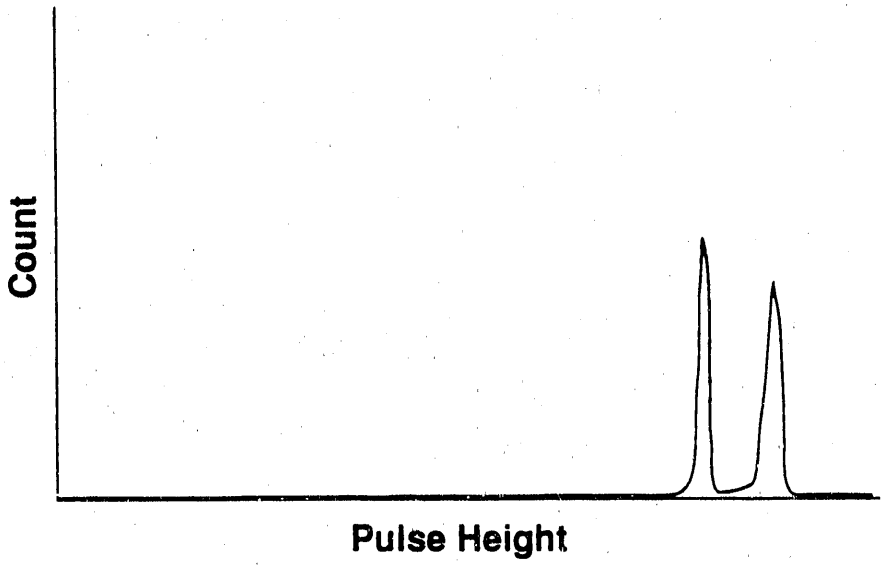

Figure A9.2 The pulse height spectrum taken with both the Cf and Am sources in place. The x-axis is proportional to energy and the y-axis is the particle count for each energy bin.

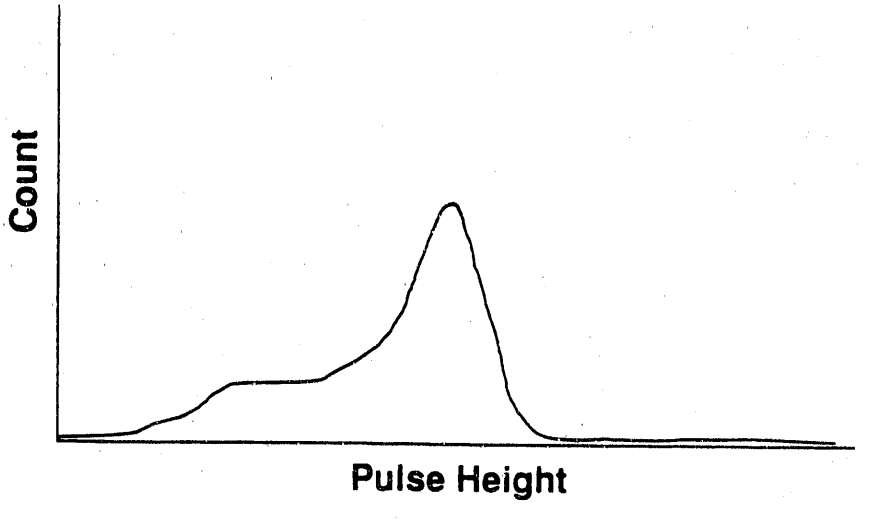

Figure A9.3 The expanded pulse height spectrum of the Am source. The shoulder on the low energy side is due to the emission of the secondary α particles.

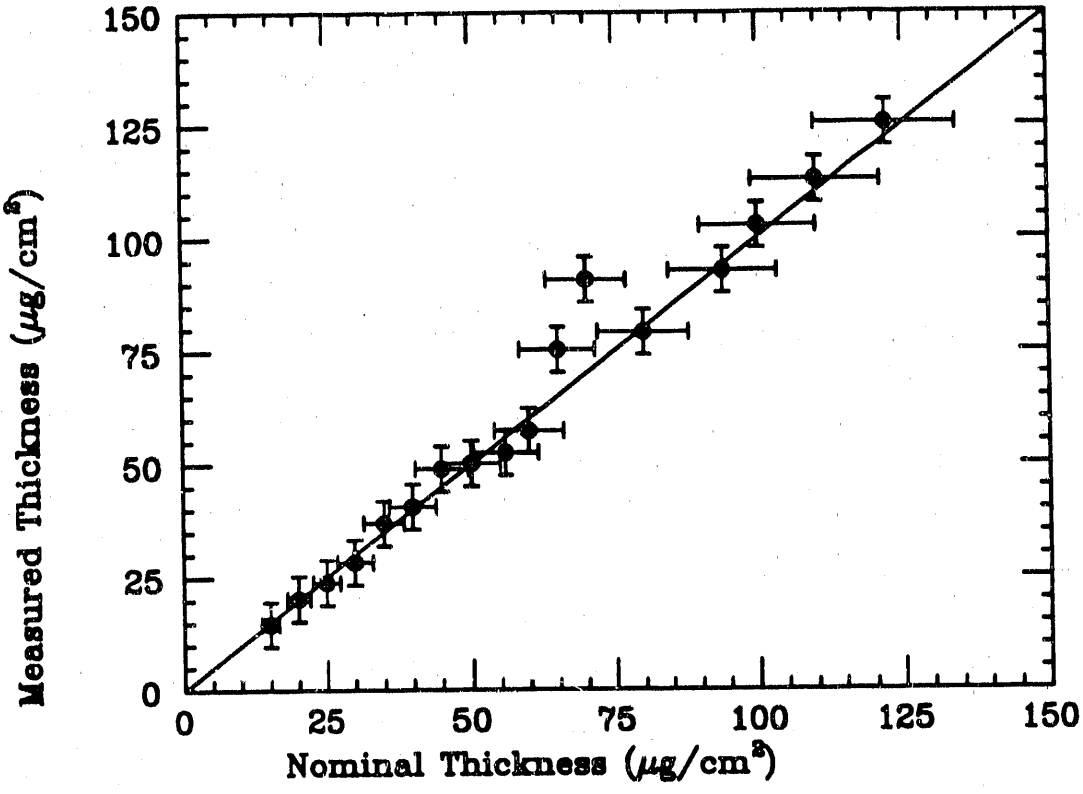

Figure A9.4 The results of the thickness measurement. The x-axis is the nominal thickness as claimed by the manufacturer. The y-axis is the thickness measured by α ranging.

APPENDIX 10

This appendix contains the data, in numerical form, for the relative yields of various excited states of hydrogen as a function of carbon foil thickness. The yield error bars are statistical only.

Table A10.1 Relative yield of n = 3 at 500 MeV.

Foil Thickness ($\mu g/cm^2$)	Uncertainty ($\mu g/cm^2$)	Yield (Arb. Units)	Error
15.0	0.6	60.0	22.0
21.0	0.8	118.0	20.0
25.0	1.0	66.0	21.0
30.0	1.2	137.0	22.0
35.0	1.4	181.0	22.0
40.0	1.6	155.0	22.0
45.0	1.8	151.0	21.0
50.0	2.0	159.0	22.0
56.0	2.2	207.0	23.0
60.0	2.4	137.0	22.0
65.0	2.6	116.0	20.0
70.0	2.8	188.0	22.0

Table A10.2 Relative yield of n = 4 at 500 MeV.

Foil Thickness ($\mu g/cm^2$)	Uncertainty ($\mu g/cm^2$)	Yield (Arb. Units)	Error
15.0	0.6	141.0	21.0
21.0	0.8	111.0	25.0
25.0	1.0	244.0	22.0
30.0	1.2	353.0	24.0
35.0	1.4	328.0	24.0
40.0	1.6	331.0	24.0
45.0	1.8	311.0	24.0
50.0	2.0	359.0	24.0
56.0	2.2	374.0	25.0
60.0	2.4	347.0	24.0
65.0	2.6	374.0	24.0
70.0	2.8	367.0	24.0

Table A10.3 Relative yield of n = 2 at 581 MeV.

Foil Thickness ($\mu g/cm^2$)	Uncertainty ($\mu g/cm^2$)	Yield (Arb. Units)	Error
15.0	0.6	2743.0	103.0
21.0	0.8	2876.0	245.0
25.0	1.0	3185.0	155.0
30.0	1.2	4226.0	208.0
35.0	1.4	3248.0	139.0
40.0	1.6	2976.0	197.0
45.0	1.8	4152.0	177.0
50.0	2.0	3433.0	93.0
56.0	2.2	2635.0	186.0
60.0	2.4	3363.0	220.0
65.0	2.6	2861.0	154.0
70.0	2.8	2634.0	169.0
80.0	3.2	2199.0	325.0
94.0	3.8	2269.0	203.0
100.0	4.0	1427.0	90.0
110.0	4.4	1798.0	131.0
122.0	4.9	1183.0	118.0

Table A10.4 Relative yield of n = 3 at 581 MeV.

Foil Thickness ($\mu g/cm^2$)	Uncertainty ($\mu g/cm^2$)	Yield (Arb. Units)	Error
15.0	0.6	360.0	38.0
21.0	0.8	458.0	27.0
25.0	1.0	487.0	41.0
30.0	1.2	659.0	53.0
35.0	1.4	783.0	43.0
40.0	1.6	795.0	44.0
45.0	1.8	845.0	40.0
50.0	2.0	996.0	64.0
56.0	2.2	995.0	65.0
60.0	2.4	977.0	57.0
65.0	2.6	1037.0	57.0
70.0	2.8	925.0	65.0
80.0	3.2	1015.0	69.0
94.0	3.8	832.0	36.0
100.0	4.0	770.0	42.0
110.0	4.4	814.0	72.0
122.0	4.9	679.0	55.0

Table A10.5 Relative yield of n = 4 at 581 MeV.

Foil Thickness ($\mu g/cm^2$)	Uncertainty ($\mu g/cm^2$)	Yield (Arb. Units)	Error
15.0	0.6	476.0	56.0
21.0	0.8	1073.0	53.0
25.0	1.0	1026.0	37.0
30.0	1.2	1549.0	59.0
35.0	1.4	1805.0	71.0
40.0	1.6	1471.0	63.0
45.0	1.8	1734.0	103.0
50.0	2.0	1661.0	58.0
56.0	2.2	1672.0	71.0
60.0	2.4	2184.0	150.0
65.0	2.6	1861.0	93.0
70.0	2.8	1837.0	126.0
80.0	3.2	1982.0	75.0
94.0	3.8	1689.0	53.0
100.0	4.0	1831.0	63.0
110.0	4.4	1528.0	71.0
122.0	4.9	1478.0	65.0

Table A10.6 Relative yield of Rydberg atoms ($12 \leq n \leq 16$) at 581 MeV.

Foil Thickness ($\mu g/cm^2$)	Uncertainty ($\mu g/cm^2$)	Yield (Arb. Units)	Error
15.0	0.6	76785.0	277.0
21.0	0.8	114639.0	339.0
25.0	1.0	135433.0	368.0
30.0	1.2	200162.0	374.0
35.0	1.4	204488.0	378.0
40.0	1.6	202740.0	450.0
45.0	1.8	204815.0	453.0
50.0	2.0	238802.0	489.0
56.0	2.2	241000.0	491.0
60.0	2.4	237965.0	488.0
65.0	2.6	254070.0	504.0
70.0	2.8	262228.0	512.0
80.0	3.2	262479.0	512.0
94.0	3.8	256789.0	507.0
100.0	4.0	260608.0	510.0
110.0	4.4	247616.0	498.0
122.0	4.9	233277.0	483.0

Table A10.7 Relative yield of n = 2 at 226 MeV.

Foil Thickness ($\mu g/cm^2$)	Uncertainty ($\mu g/cm^2$)	Yield (Arb. Units)	Error
15.0	0.6	21230.0	772.0
21.0	0.8	20235.0	727.0
25.0	1.0	17530.0	674.0
30.0	1.2	12910.0	559.0
35.0	1.4	14425.0	861.0
40.0	1.6	14850.0	856.0
45.0	1.8	15530.0	871.0
50.0	2.0	13250.0	778.0
56.0	2.2	13665.0	562.0
60.0	2.4	8050.0	367.0
65.0	2.6	8140.0	376.0
70.0	2.8	8200.0	369.0
80.0	3.2	6415.0	516.0
94.0	3.8	4210.0	345.0
100.0	4.0	3080.0	264.0
110.0	4.4	2900.0	208.0

Table A10.8 Relative yield of n = 2 at 716 MeV.

Foil Thickness ($\mu g/cm^2$)	Uncertainty ($\mu g/cm^2$)	Yield (Arb. Units)	Error
19.0	0.8	518.1	33.2
25.0	1.0	615.6	39.6
30.0	1.2	675.7	48.0
35.0	1.4	661.3	39.8
40.0	1.6	667.7	41.1
45.0	1.8	635.7	40.8
50.0	2.0	632.0	31.9
55.0	2.2	546.1	34.0
60.0	2.4	526.9	40.5
65.0	2.6	510.1	37.3
70.0	2.8	542.3	35.2
89.0	3.6	440.7	28.0
110.0	4.4	348.6	18.7
122.0	4.9	227.6	16.2
159.0	6.4	166.1	14.4
198.0	7.9	142.7	11.0

Table A10.9 Relative yield of n = 1 at 800 MeV.

Foil Thickness ($\mu g/cm^2$)	Uncertainty ($\mu g/cm^2$)	Yield (Arb. Units)	Error
19.0	0.8	22189.0	909.0
25.0	1.0	26895.0	1093.0
30.0	1.2	29545.0	1002.0
35.0	1.4	29161.0	939.0
40.0	1.6	28063.0	1012.0
45.0	1.8	27348.0	928.0
50.0	2.0	26581.0	1201.0
55.0	2.2	27575.0	861.0
60.0	2.4	27958.0	1349.0
65.0	2.6	26477.0	1121.0
70.0	2.8	24455.0	893.0
89.0	3.6	21666.0	1224.0
110.0	4.4	17030.0	901.0
122.0	4.9	13997.0	661.0
159.0	6.4	9064.0	369.0
198.0	7.9	7669.0	394.0

Table A10.10 Relative yield of n = 2 at 800 MeV.

Foil Thickness ($\mu g/cm^2$)	Uncertainty ($\mu g/cm^2$)	Yield (Arb. Units)	Error
19.0	0.8	100.3	4.8
25.0	1.0	113.5	5.0
30.0	1.2	125.3	5.7
35.0	1.4	128.9	6.2
40.0	1.6	131.6	5.9
45.0	1.8	148.7	6.1
50.0	2.0	134.0	6.2
55.0	2.2	151.0	6.9
60.0	2.4	133.8	5.8
65.0	2.6	96.8	4.8
70.0	2.8	115.9	5.3
89.0	3.6	84.5	3.9
110.0	4.4	69.3	3.4
122.0	4.9	69.6	3.1
159.0	6.4	35.2	1.8
198.0	7.9	31.1	1.8

Table A10.11 Relative yield of n = 3 at 800 MeV.

Foil Thickness ($\mu g/cm^2$)	Uncertainty ($\mu g/cm^2$)	Yield (Arb. Units)	Error
19.0	0.8	11.01	0.48
25.0	1.0	11.78	0.43
30.0	1.2	19.54	0.75
35.0	1.4	18.83	0.69
40.0	1.6	22.18	0.71
45.0	1.8	19.73	0.67
50.0	2.0	21.15	0.70
55.0	2.2	22.93	0.72
60.0	2.4	23.75	0.67
65.0	2.6	23.50	0.87
70.0	2.8	23.24	0.73
89.0	3.6	24.09	0.82
110.0	4.4	23.69	0.78
122.0	4.9	16.94	0.85
159.0	6.4	14.93	0.69
198.0	7.9	11.57	0.46

Table A10.12 Relative yield of n = 4 at 800 MeV.

Foil Thickness ($\mu g/cm^2$)	Uncertainty ($\mu g/cm^2$)	Yield (Arb. Units)	Error
25.0	1.0	2.81	0.13
30.0	1.2	4.13	0.23
35.0	1.4	4.31	0.17
40.0	1.6	4.82	0.21
45.0	1.8	4.63	0.30
50.0	2.0	4.69	0.31
55.0	2.2	5.27	0.18
60.0	2.4	5.42	0.21
65.0	2.6	5.80	0.20
89.0	3.6	6.30	0.20
110.0	4.4	5.58	0.24
122.0	4.9	5.52	0.19
159.0	6.4	3.80	0.22
198.0	7.9	3.78	0.18

Table A10.13 Relative yield of n = 5 at 800 MeV.

Foil Thickness ($\mu g/cm^2$)	Uncertainty ($\mu g/cm^2$)	Yield (Arb. Units)	Error
19.0	0.8	0.655	0.046
25.0	1.0	0.850	0.051
30.0	1.2	1.210	0.068
35.0	1.4	1.189	0.055
40.0	1.6	1.098	0.073
45.0	1.8	1.212	0.070
50.0	2.0	1.374	0.064
55.0	2.2	1.516	0.069
60.0	2.4	1.637	0.067
65.0	2.6	1.473	0.081
70.0	2.8	1.527	0.064
89.0	3.6	1.653	0.086
110.0	4.4	1.746	0.082
122.0	4.9	1.273	0.082
159.0	6.4	1.141	0.062
198.0	7.9	1.037	0.058

Table A10.14 Relative yield of n = 10 at 800 MeV.

Foil Thickness ($\mu g/cm^2$)	Uncertainty ($\mu g/cm^2$)	Yield (Arb. Units)	Error
19.0	0.8	4387.0	367.0
25.0	1.0	4368.0	367.0
30.0	1.2	6021.0	500.0
35.0	1.4	5571.0	400.0
40.0	1.6	5690.0	401.0
45.0	1.8	5912.0	450.0
50.0	2.0	5488.0	420.0
55.0	2.2	5810.0	520.0
60.0	2.4	6334.0	530.0
65.0	2.6	6766.0	630.0
70.0	2.8	6634.0	509.0
89.0	3.6	7415.0	510.0
110.0	4.4	7635.0	530.0
122.0	4.9	7420.0	573.0
159.0	6.4	5755.0	695.0
198.0	7.9	5670.0	716.0
303.0	12.1	2777.0	600.0

Table A10.15 Relative yield of n = 11 at 800 MeV.

Foil Thickness ($\mu g/cm^2$)	Uncertainty ($\mu g/cm^2$)	Yield (Arb. Units)	Error
19.0	0.8	1968.0	90.7
25.0	1.0	2867.0	87.6
30.0	1.2	3913.5	109.2
35.0	1.4	3838.0	107.9
40.0	1.6	3687.0	120.3
45.0	1.8	3984.0	117.2
50.0	2.0	4350.0	42.1
55.0	2.2	4354.0	119.9
60.0	2.4	4009.0	105.3
65.0	2.6	4654.0	129.7
70.0	2.8	4949.0	116.4
89.0	3.6	5001.0	157.2
110.0	4.4	4041.0	124.9
122.0	4.9	4637.0	144.1
159.0	6.4	3783.0	121.6
198.0	7.9	3409.0	137.7
303.0	12.1	1409.0	49.3

References

1. M. H. Shariflan-Attar, Ph.D. Dissertation, University of New Mexico, 1977.

2. H. C. Bryant *et al.*, Phys. Rev. Lett. **28**, 228 (1977).

3. G. H. Tootoonchi-Sarraf, Ph.D. Dissertation, University of New Mexico, 1977.

4. P. A. M. Gram *et al.*, Phys. Rev. Lett. **40**, 107 (1978).

5. M. E. Hamm *et al.*, Phys. Rev. Lett. **43**, 1715 (1979).

6. Charles A. Frost, Ph.D. Dissertation, University of New Mexico; Published as Los Alamos National Lab. Report No. LA-8976-T (1981).

7. J. B. Donahue *et al.*, Phys. Rev. Lett. **48**, 1538 (1982).

8. E. P. Wigner, Phys. Rev. 73, 9, 1002 (1948).

9. G. H. Wannier, Phys. Rev. 90, 817 (1953).

10. Kenneth B. Butterfield, Ph.D. Dissertation, University of New Mexico; Published as LANL Report No. LA-10149-T (1984).

11. Stanley Cohen, Ph.D. Dissertation, University of New Mexico; Published as LANL Report No. LA-10726-T (1986).

12. S. Cohen, *et al.*, Phys Rev A, 36, 4728 (1987).

13. H. C. Bryant *et al.*, Phys. Rev. Lett. **58**, 2412 (1987).

14. I. I. Fabrikant, Sov. Phys. JETP **52**, 1045 (1980).

15. W. P. Reinhardt, Atomic Excitation and Recombination in External Fields, M. H. Nayfeh and C. W. Clark, Eds. (Gordon and Breach, 1985) page 85.

16. A. R. P. Rau and H. Wong, Phys. Rev. A **37**, 632 (1988).

17. Du and Delos, Phys. Rev. A **38**, 5609 (1988).

18. H. C. Bryant, Atomic Spectra and Collisions in External Fields II, Royal Holloway and Bedford New College (1987).

19. W. W. Smith, in Atomic Excitation and Recombination in External Fields, M. H. Nayfeh and C. W. Clark, Eds. (Gordon and Dreach, 1985).

20. D. W. MacArthur *et al.*, Phys. Rev. Lett. **56**, 282 (1986).

21. C. Y. Tang *et al.* Phys. Rev. Lett. **39**, 6068 (1989).

22. Hans A. Bethe and Edwin Salpeter, Quantum Mechanics of One- and Two-electron Atoms, (Academic Press, New York, 1957).

23. H. A. Bethe: Z. Physik **57**, 815 (1929).

24. A. van Wijngaarden *et al.*, Phys. Rev. A **32**, 2150 (1985).

25. U. Fano and R. A. P. Rau, Atomic Collisions and Spectra (Academic, Orlando, 1986).

26. T. G. Eck, Phys. Rev. Lett. **33**, 1055 (1974).

27. Y. Yamazaki *et al.*, Phys. Rev. Lett. **61**, 2913 (1988).

28. Joachim Burgdorfer and Chris Bottcher, Phys. Rev. Lett. **61**, 2917 (1988).

29. W. Brandt, in Atomic Collisions in Solids, edited by S. Datz, B. Appleton, and C. Moak (Plenum, New York, 1975), p. 761.

30. D. P. Almeida, *et al.*, Phys. Rev. A **36**, 16 (1987).

31. K. Dybdal *et al.*, Nucl. Instrum. Methods Phys. Res. **B13**, 581 (1986).

32. June Davidson, Phys. Rev. A **12**, 1350 (1975).

33. T. Aberg and O. Goscinki, Phys. Rev. A **24**, 801 (1982).

34. C. J. Anderson, *et al.*, Phys. Rev. A **22**, 822 (1980).

35. N. H. Tolk, *et al.*, Nucl. Instrum. Methods **202**, 247 (1982).

36. J. D. Garcia, Nucl. Instrum. Methods **90**, 295 (1970).

37. Donald J. Liska, LANL Report No LA-4795-MS (1971).

38. V. A. Bazylev and A. V. Demura, *Phys. Lett.*, 91A, No. 7, 369 (1982).

39. A. J. Jason, *et al.*, LANL Report No. LA-UR-81-831, (1981).

40. T. F. Gallagher, Rep. Prog. Phys. **51**, p. 154 (1988).

41. E. J. Galvez, *et al.*, Phys. Rev. Lett. **61**, 2011 (1988).

42. Q. Su, *et al.*, Phys. Rev. Lett. **64**, 862 (1990).

43. M. Font, Phys. Rev. A **40)**, 5659 (1990).

44. J. N. Knudson, LANL Report No MP-7-TN-23 (1990).

45. P. G. Harris, *et al.*, Accepted for publication by Nucl. Instrum. Methods A (1990).

46. J. C. Allred *et al.*, LANL Report No LA-UR-87-327 (1987).

47. H. C. Bryant *et al.*, Phys. Rev. Lett. **27**, 1928 (1971).

48. H. C. Bryant, Private Communication (1989).

49. A. P. Freach, Special Relativity, The MIT Introdcutory Physics Series, W. W. Norton & Company, New York, (1968).

50. W. E. Meyerhof, *et al.*, Panel Report on "Relativistic Atomic Collisions", Workshop on future opportunities in AMO sciences, Lawrence Berkeley Laboratory (1989).

51. Group MP-1, Q Document MP-1-3417-1, LAMPF (1985).

52. Group MP-1, Q Document MP-1-3401-5, LAMPF (9186).

53. R. C. Fernow, Introduction to Experimental High Energy Physics, Cambridge University Press, New York (1986).

54. J. W. B. Hughes, Proc. Phys. Soc., 91, 810 (1967).

55. R. J. Damburg and V. V. Kolosov, "Rydberg states of atoms and molecules", Chapter 3, Edited by R. F. Stebbings, Cambridge Univ. Press (1983).

56. R. A. Reeder, LANL Technical Note At-2-BS, (1986).

57. B. H. Bransden and C. J. Joachain, Physics of Atoms and Molecules, Longman Publishing Company, New York (1984).

58. Hans A. Bethe and Edwin Salpeter, Quantum Mechanics of One- and Two-electron Atoms, Academic Press, New York (1957).

59. J. R. Taylor, An Introduction to Error Analysis, University Science Books, Mill Valley, California (1982).

60. LAMPF Data Analysis Center, MINUIT Under VAX/VMS, Office Memorandum, March 15 (1979).

61. Arizona Carbon Foil Co., Inc., Tucson, Arizona (1989).

62. H. P. Robertson, Rev. Mod. Phys. **21**, 378 (1949).

63. P. G. Harris, Private Communication (1990).

64. W. H. Press, *et al.*, "Numerical Recipies", Cambridge Univ. Press (1986).

65. P. G. Harris, Ph.D. Dissertation, University of New Mexico, 1990.

66. C. Y. Tang, Ph.D. Dissertation, University of New Mexico, 1990.

67. U. Fano, R. A. P. Rau, Atomic Collisions ans Spectra, Acadamic, Orlando, Section 7.2.4 (1986).

68. T. J. Broad and W. P. Reinhardt, Phys. Rev A **14**, 2159 (1976).

69. A. R. P. Rau, Phys. Rev. A **4**, 207 (1971).

70. B. H. Armstrong, Phys. Rev. 131, 1132 (1963).

71. G. F. Drukarev, Sov. Phys. JETP, 31, No. 6, 1193 (1970).

•U S GOVERNMENT PRINTING OFFICE 1990-0-773-034 20094

END

DATE FILMED

11/02/90